ELECTRONIC SUPPLEMENTARY INFORMATION (ESI)

# Effect of extended π-surface and N-butyl substituents of imidazoles on the reactivity, electrochemical behaviours and biological interactions of corresponding Pt(II)-C^N^C pincer carbene complexes; Exploring DFT and docking interactions.

Rajesh Bellam*[a], Daniel Omondi Onunga[a,b], Deogratius Jaganyi[c,d], Ross Robinson[a] and Allen Mambanda[a]

[a]School of Chemistry and Physics, University of KwaZulu-Natal, Private Bag X01, Scottsville, Pietermaritzburg 3209, South Africa.
[b]Department of Chemistry, Maseno University, Maseno, Kenya.
[c]School of Pure and Applied Sciences, Mount Kenya University, Thika, Kenya.
[d]Department of Chemistry, Durban University of Technology, P.O. Box 1334, Durban 4000, South Africa.

*Rajesh Bellam: rajeshchowdarybellam@gmail.com

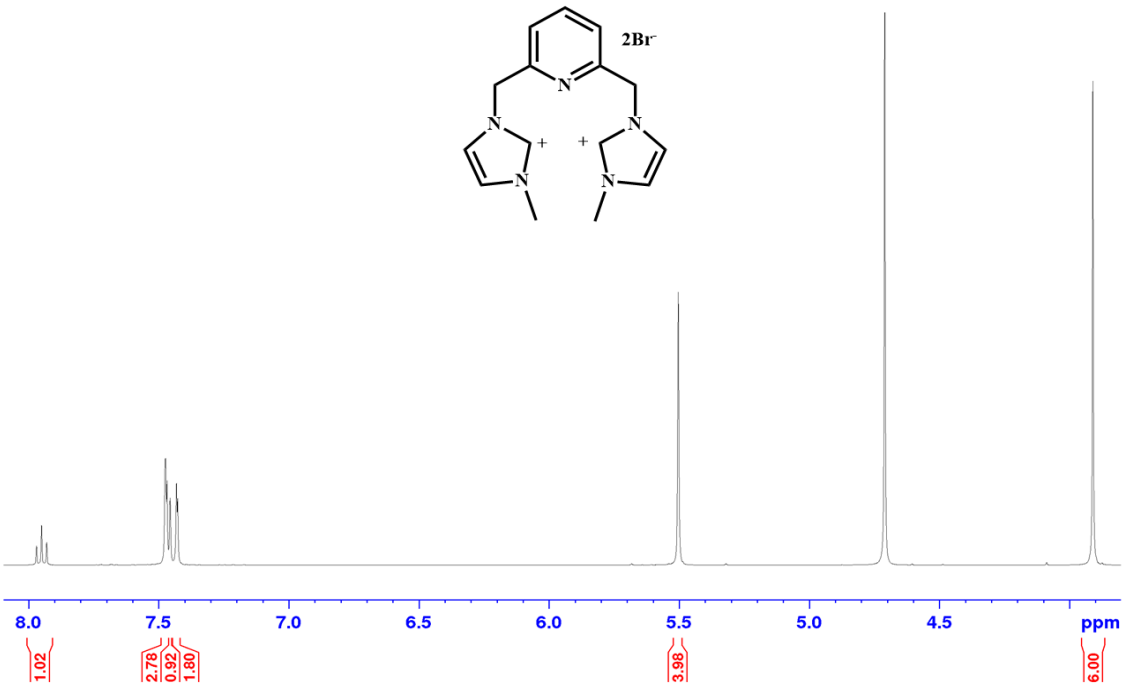


**Fig. S1:** $^{1}$H NMR spectrum of 2,6-bis[(3-methylimidazolium-1-yl)methyl]pyridine; **$L_1$** (400 MHz, $(CD_3)_2SO$).

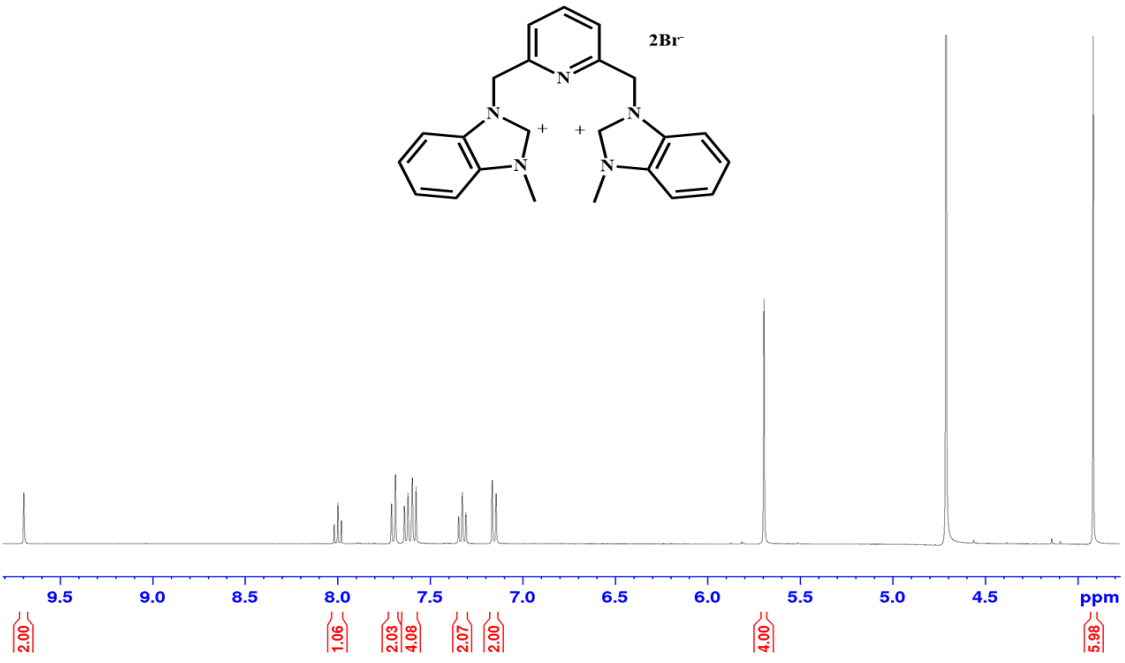


**Fig. S2:** $^{1}$H NMR spectrum of 2,6-bis[(3-methylbenzimidazol-1-yl)methyl]pyridine; **$L_2$** (400 MHz, $(CD_3)_2SO$).

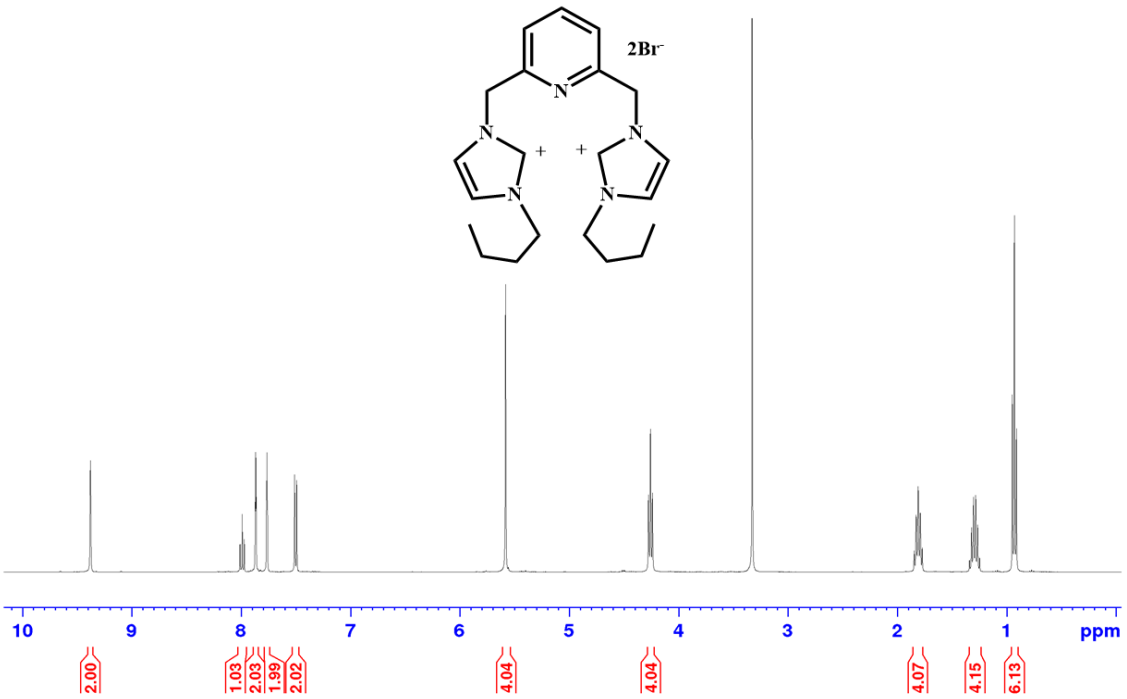


**Fig. S3:** $^{1}$H NMR spectrum of 2,6-bis[(3-butylimidazol -1-yl)methyl]pyridine; **$L_3$** (400 MHz, $(CD_3)_2SO$).

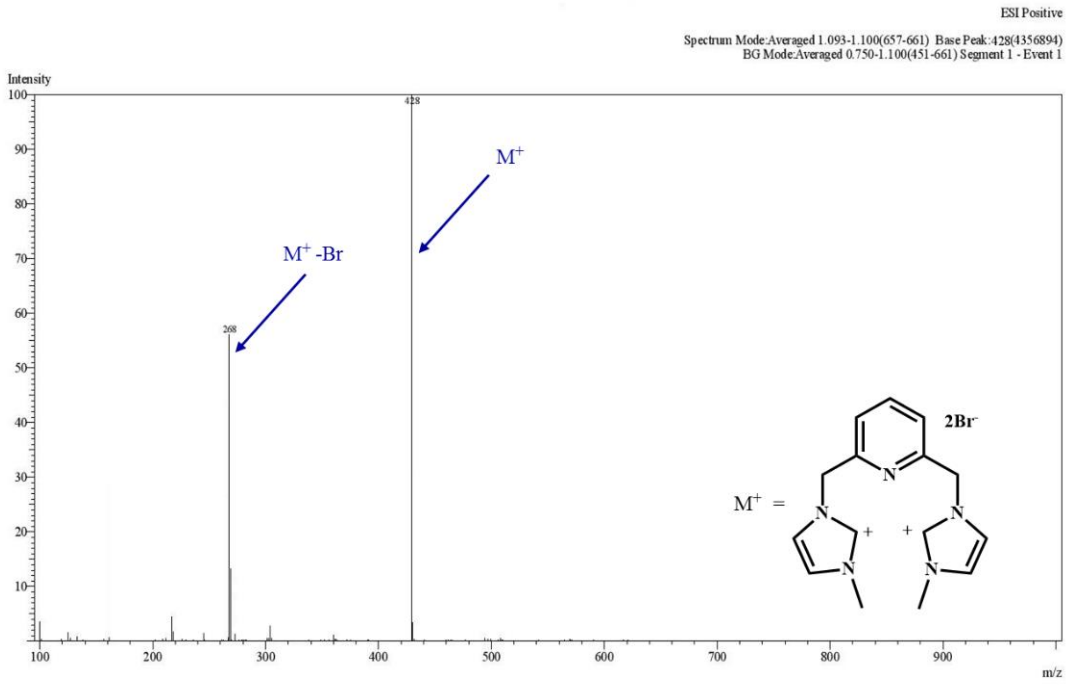


**Fig. S4:** TOF-MS spectra of 2,6-bis[(3-methylimidazolium-1-yl)methyl]pyridine; **$L_1$**

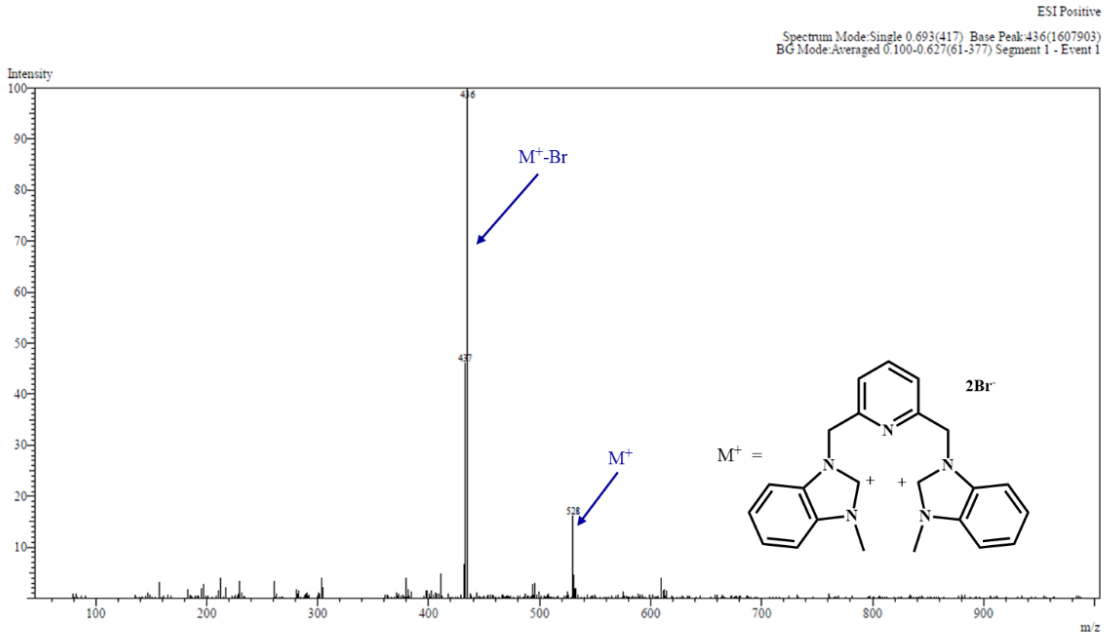


**Fig. S5:** TOF-MS spectra of 2,6-bis[(3-methylbenzimidazol-1-yl)methyl]pyridine; **$L_2$**

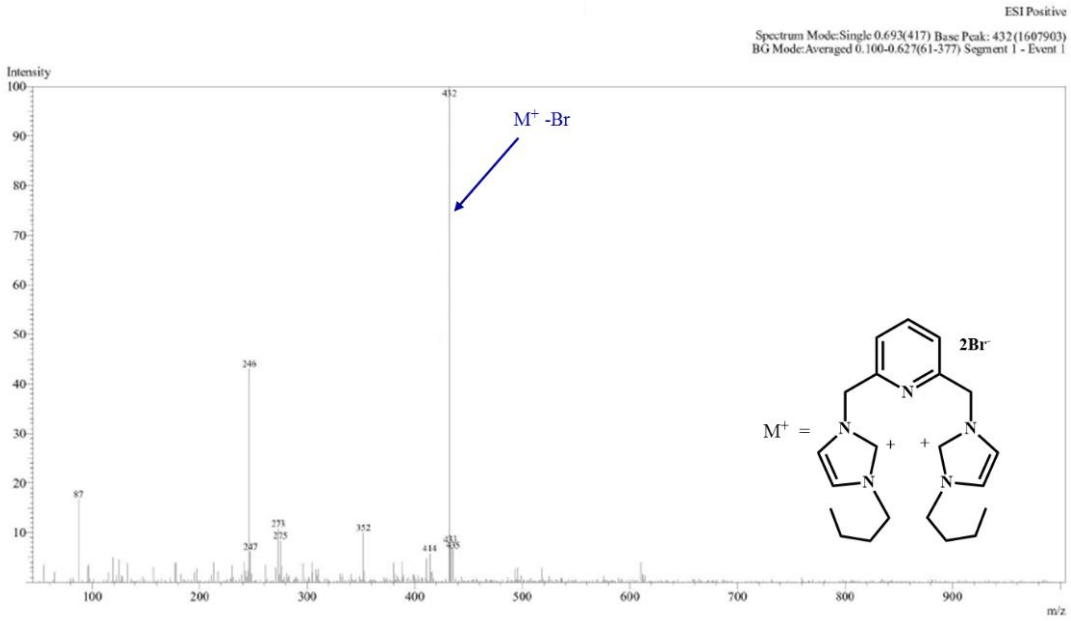


**Fig. S6:** TOF-MS spectra of 2,6-bis[(3-butylimidazol -1-yl)methyl]pyridine; **$L_3$**

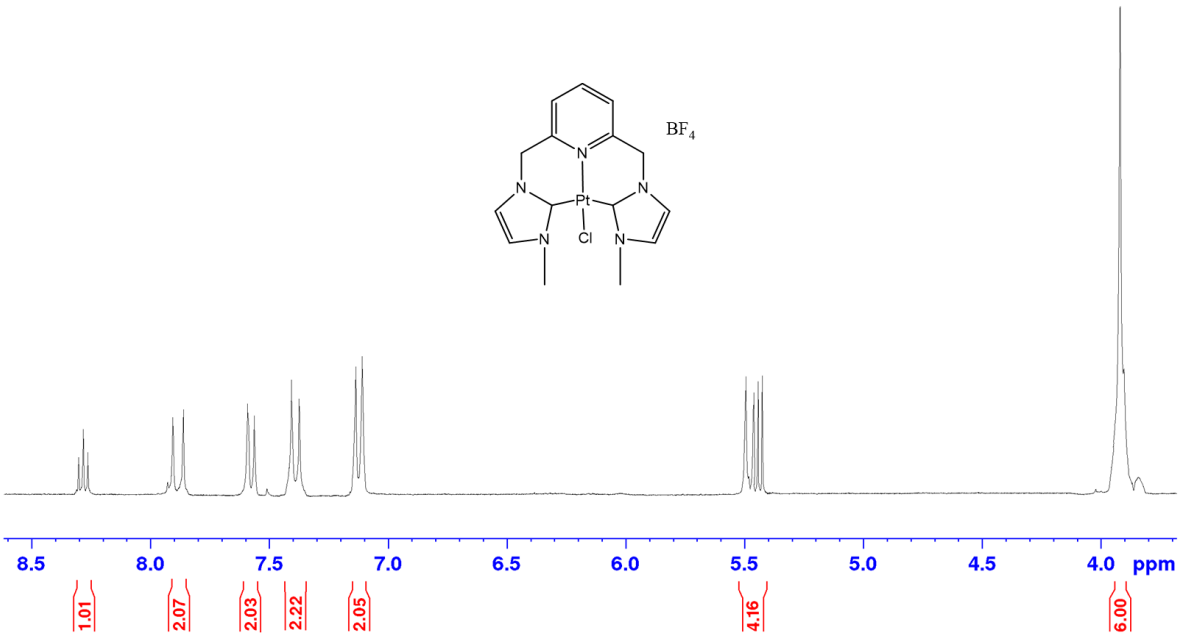


**Fig. S7:** $^{1}$H NMR spectrum of 2,6-bis[(3-methylimidazolium-1-yl)methyl]pyridine platinum(II) chloride tetrafluoroborate; **$PtL_1$** (400 MHz, $(CD_3)_2SO$).

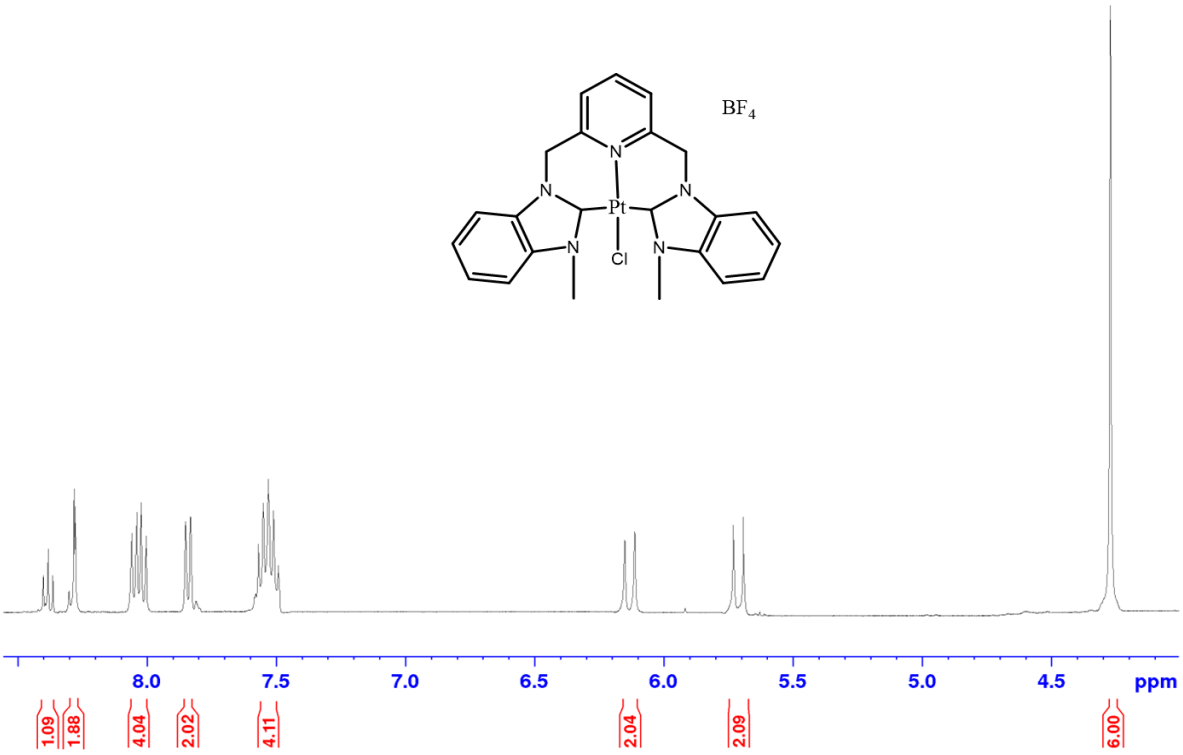


**Fig. S8:** $^{1}$H NMR spectrum of 2,6-bis[(3-methylbenzimidazol-1-yl)methyl]pyridine platinum(II) chloride tetrafluoroborate; **$PtL_2$** (400 MHz, $(CD_3)_2SO$).

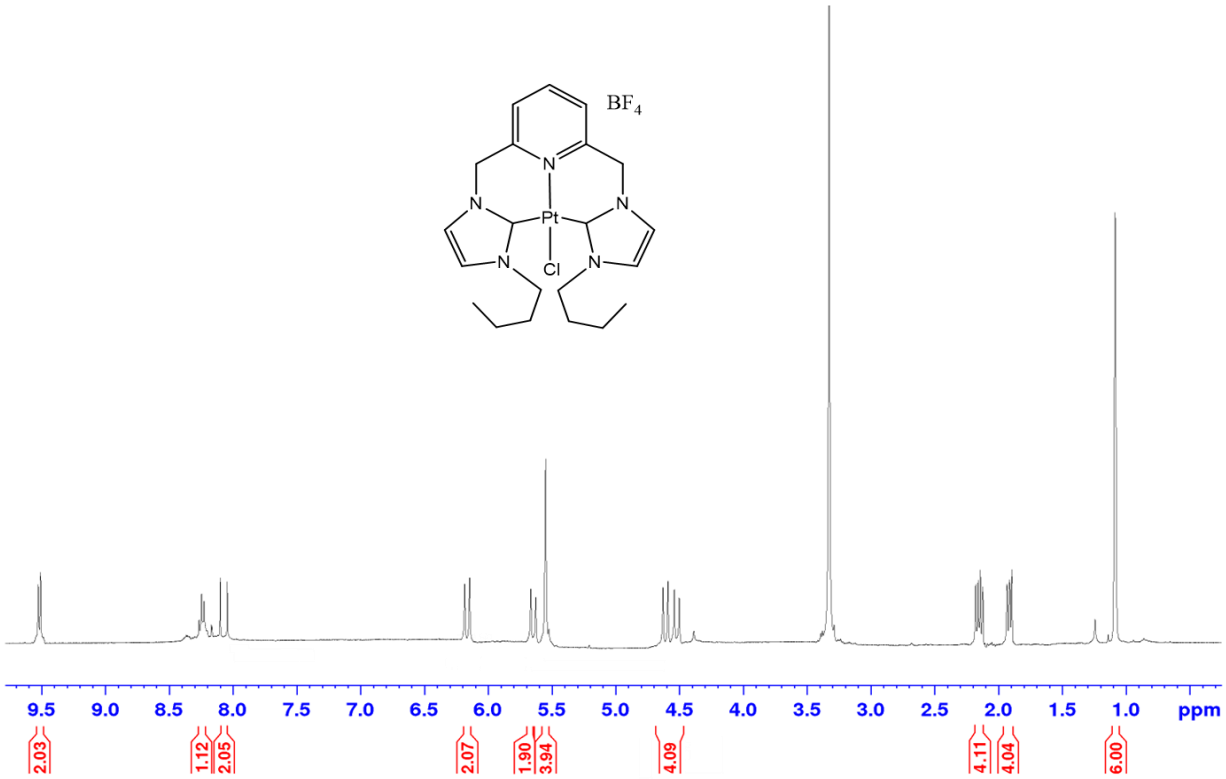


**Fig. S9:** $^{1}$H NMR spectrum of 2,6-bis[(3-butylimidazol -1-yl)methyl]pyridine platinum(II) chloride tetrafluoroborate, **$PtL_3$** (400 MHz, $(CD_3)_2SO$).

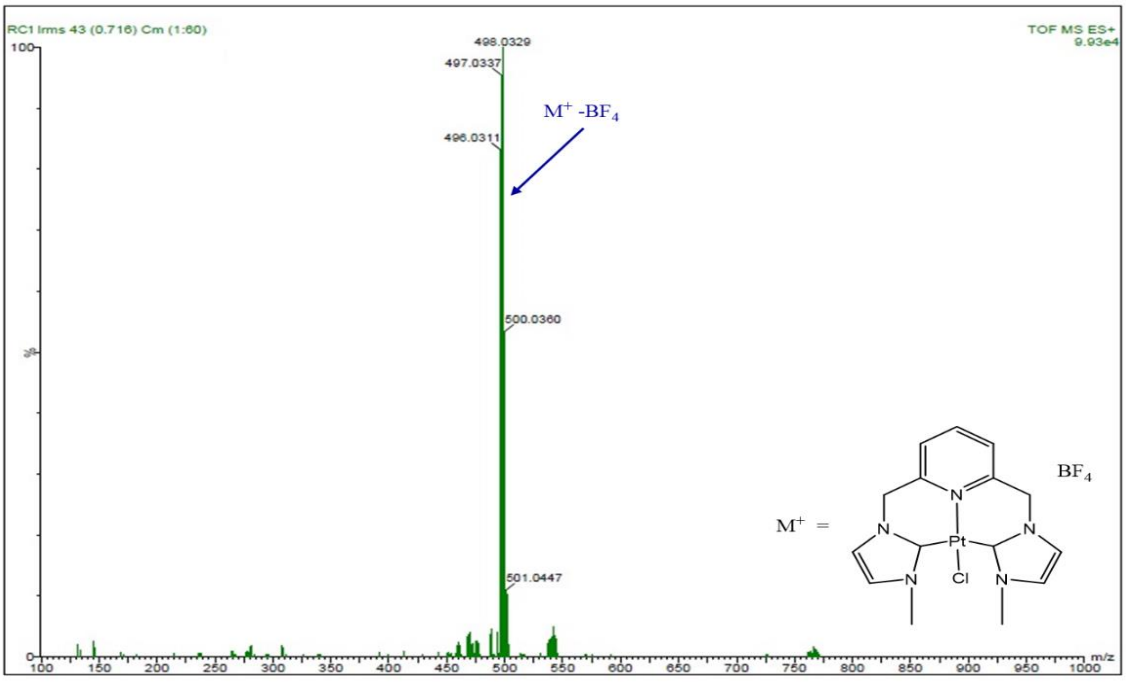


**Fig. S10:** TOF-MS spectra of 2,6-bis[(3-methylimidazolium-1-yl)methyl]pyridine platinum(II) chloride tetrafluoroborate complex; **$PtL_1$**.

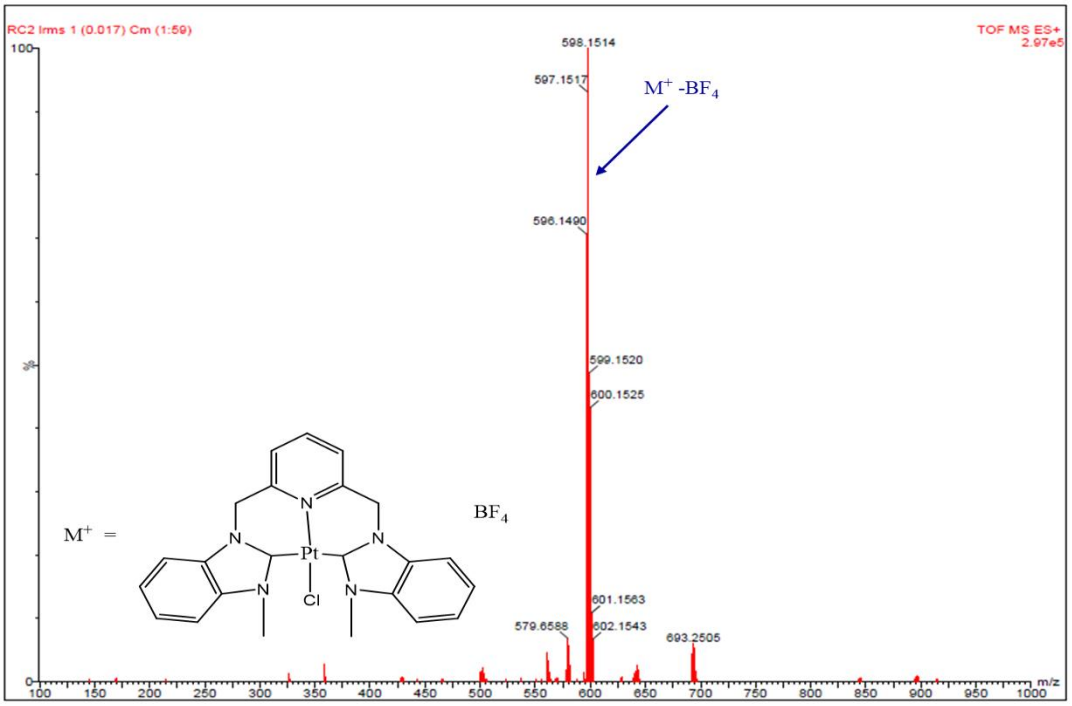


**Fig. S11:** TOF-MS spectra of 2,6-bis[(3-methylbenzimidazol-1-yl)methyl]pyridine platinum(II) chloride tetrafluoroborate complex; **$PtL_2$**.

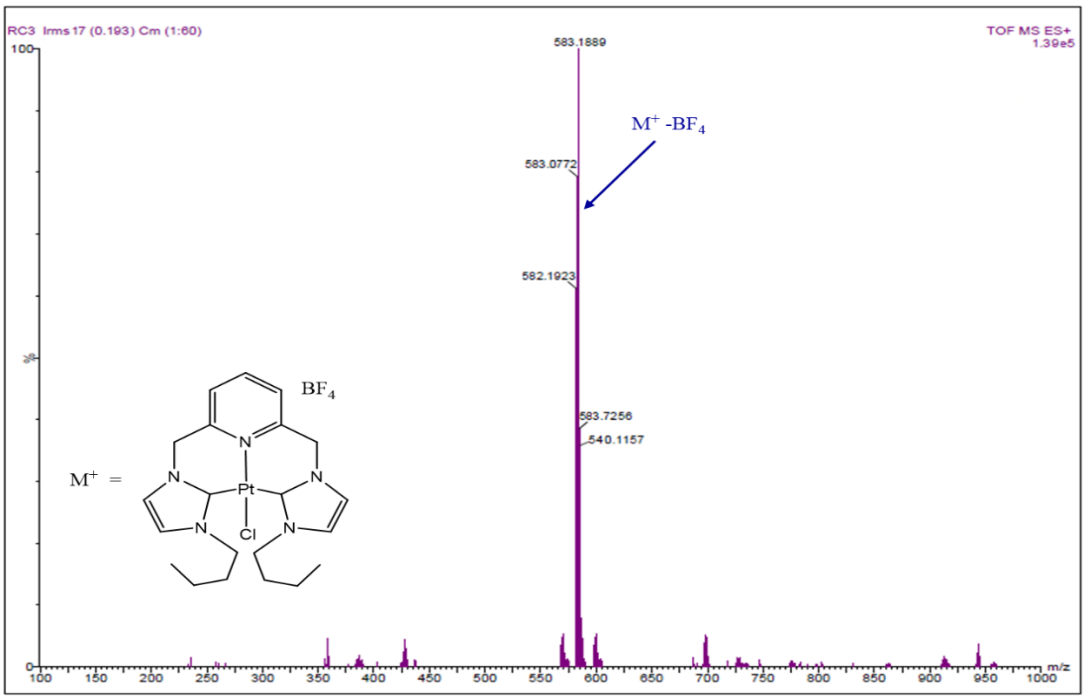


**Fig. S12:** TOF-MS spectra of 2,6-bis[(3-butylimidazol -1-yl)methyl]pyridine platinum(II) chloride tetrafluoroborate complex; **$PtL_3$**.

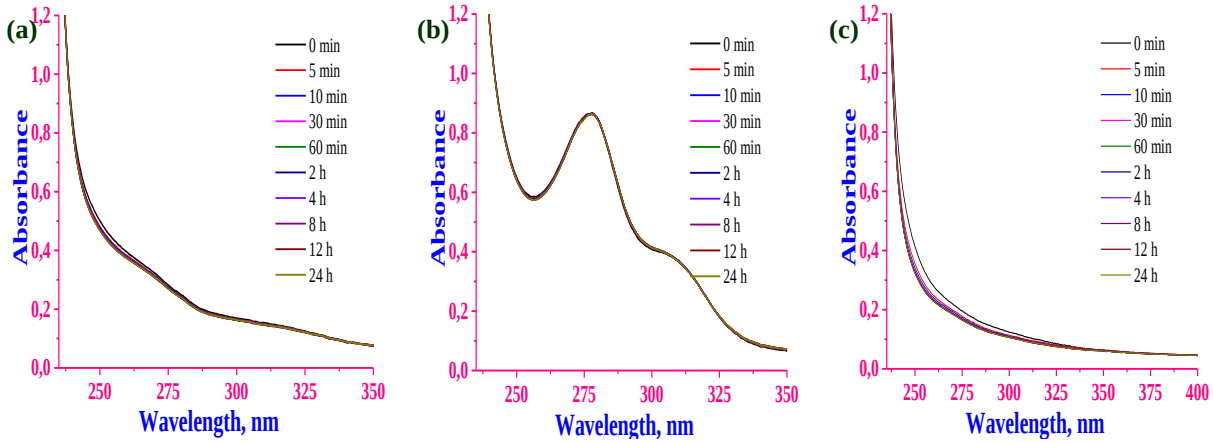


**Fig. S13:** UV–Vis spectra of complexes **PtL$_1$** (a), **PtL$_2$** (b) and **PtL$_3$** (c) in Tris-HCl/50 mM NaCl buffer (pH = 7.2) over a 24 h period. [**PtL$_1$**/**PtL$_2$**/**PtL$_3$**] = 5.0 x $10^{-5}$ M and T = 35 °C.

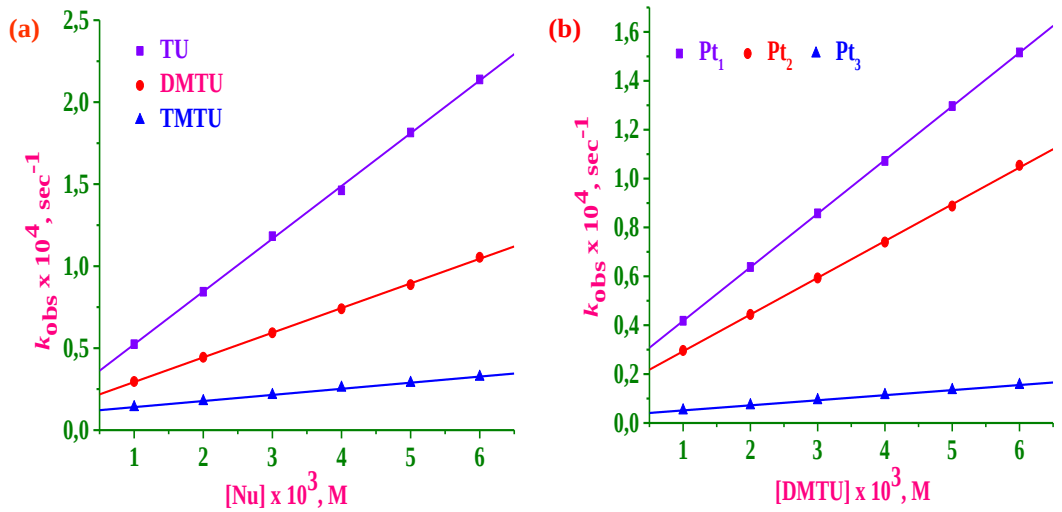


**Fig. S14** Linear plots of $k_{obs}$ versus [Nu] for the reaction of **PtL$_2$** with Nu (a) and for the reactions with three Pt(II) C^N^C pincer complexes (**PtL$_1$**, **PtL$_2$** and **PtL$_3$**) with dmtu (b): [**PtL$_1$**/ **PtL$_2$**/ **PtL$_3$**] = 50 µM, pH = 7.2 (Tris-HCl/50 mM NaCl) and T = 35 °C.

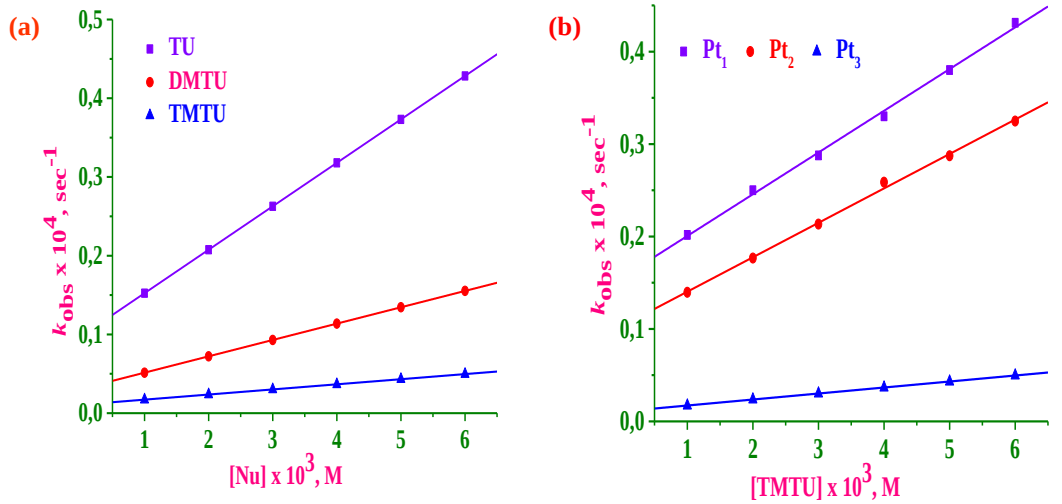


**Fig. S15** Linear plots of $k_{obs}$ versus [Nu] for the reaction of **PtL$_3$** with Nu (a) and for the reactions with three Pt(II) C^N^C pincer complexes (**PtL$_1$**, **PtL$_2$** and **PtL$_3$**) with tmtu (b): [**PtL$_1$**/ **PtL$_2$**/ **PtL$_3$**] = 50 µM, pH = 7.2 (Tris-HCl/50 mM NaCl) and T = 35 °C.

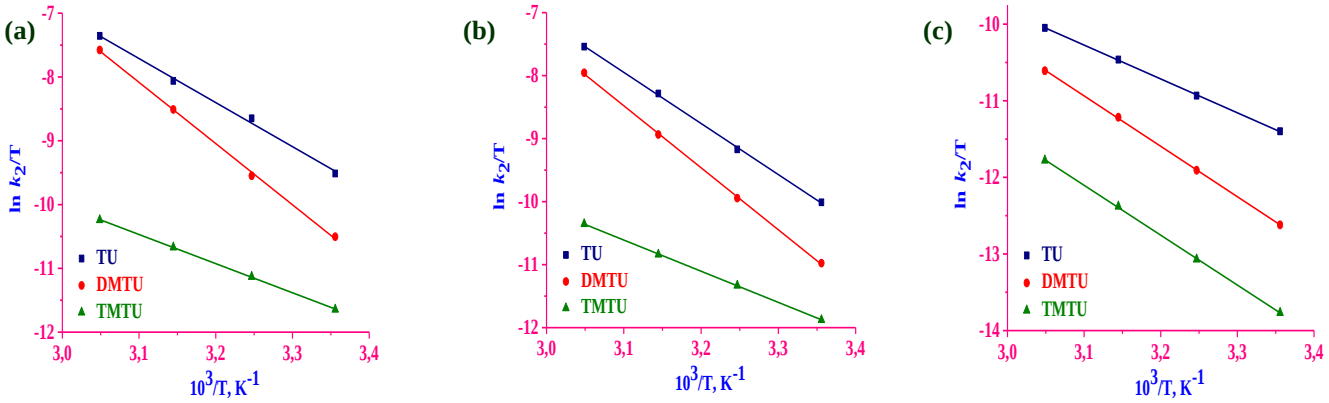


**Fig. S16** Eyring plots for the substitution of chloride from **$PtL_1$** (a), **$PtL_2$** (b) and **$PtL_3$** (c) by TU nucleophiles.

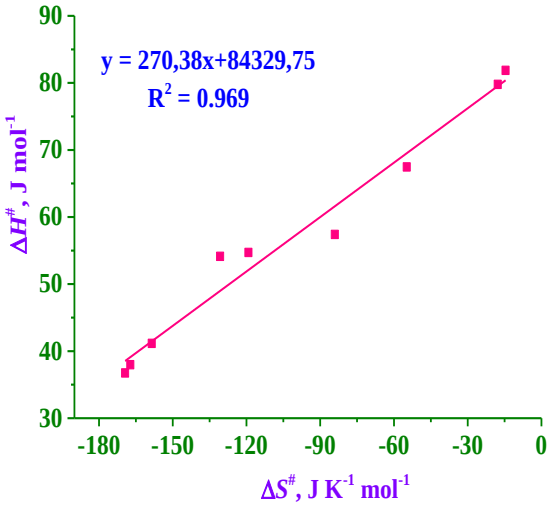


**Fig. S17** *Iso*-kinetic plots for the substitution of chloride ligands by Nu of all the three Pt(II) C^N^C pincer complexes.

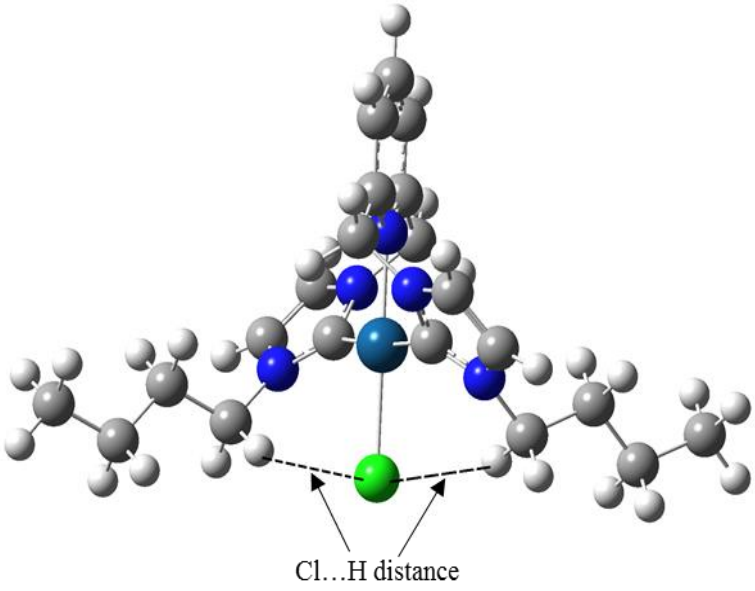


**Fig. S18** DFT optimized structure of **$PtL_3$** representing chlorine *ipso* hydrogen lengths.

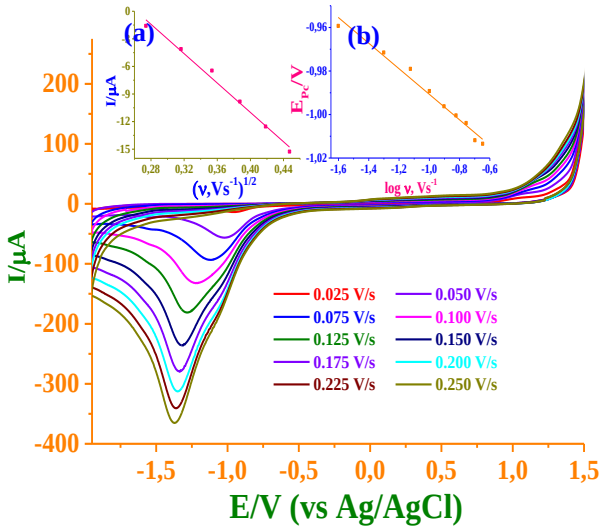


**Fig. S19** Effect of scan rate on the CV for 1.0 mM of **$PtL_2$** at the different scan rates from 25 to 250 mV/s. Insets: (a) Relationship between reduction peak currents ($I_{pc}$) and the square root of scan rate (v); (b) linear relationship between the reduction peak potential ($E_{pc}$) and the logarithm of scan rate.

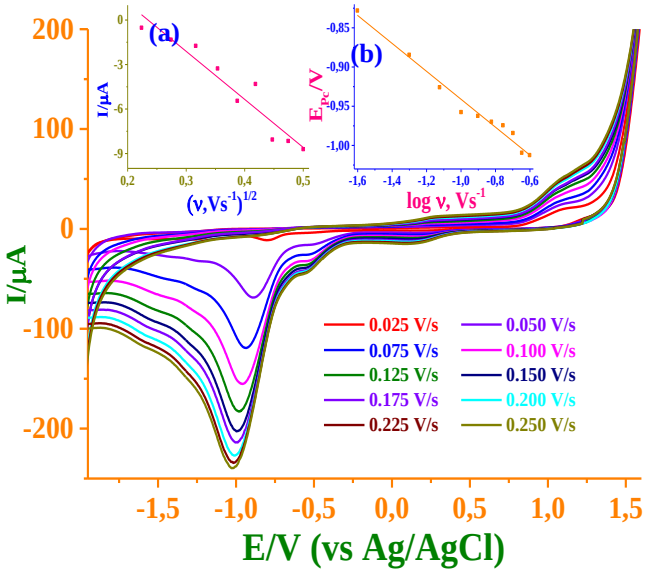


**Fig. S20** Effect of scan rate on the CV for 1.0 mM of **$PtL_3$** at the different scan rates from 25 to 250 mV/s. Inset: (a) Relationship between reduction peak currents ($I_{pc}$) and the square root of scan rate (v); (b) linear relationship between the reduction peak potential ($E_{pc}$)and the logarithm of scan rate.

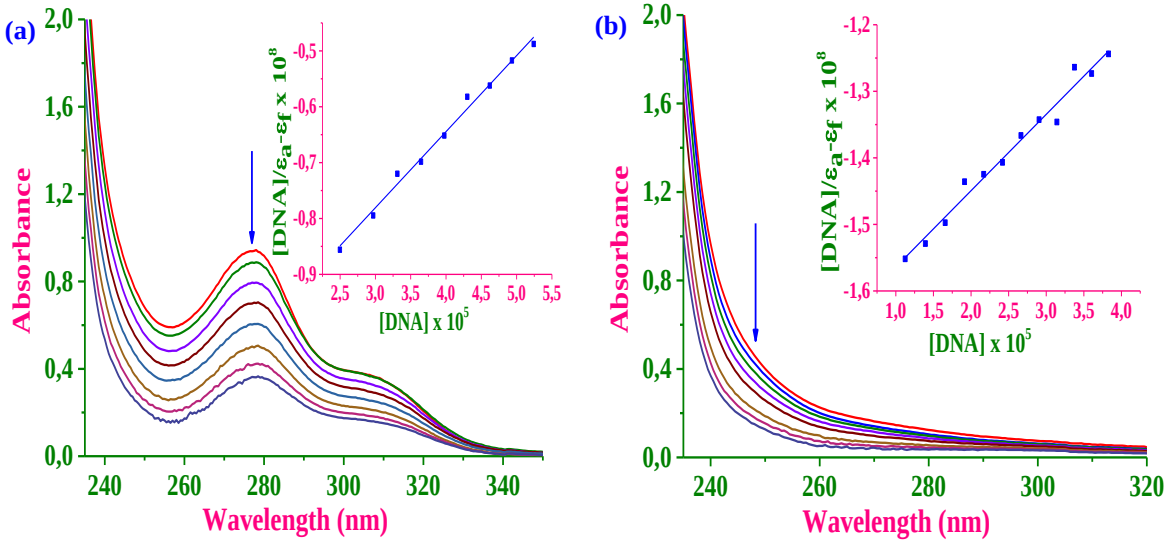


**Fig. S21** Absorption spectra of 48 µM of **$PtL_2$** (a) and **$PtL_3$** (b) in 5 mM Tris-HCl/50 mM buffer at pH 7.2 upon addition of CT-DNA (0 - 40 µM). The arrow shows the change in absorbance upon increasing the CT-DNA concentration. Inset: Wolfe-Shimer plot of [CT-DNA] versus [DNA]/($\varepsilon_a$- $\varepsilon_f$).

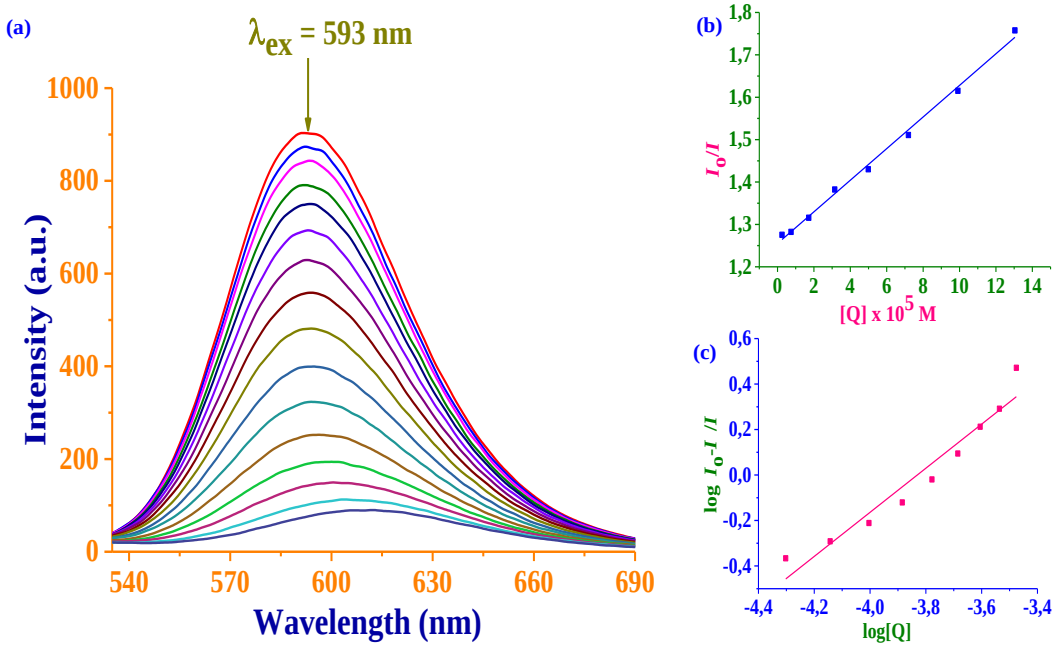


**Fig. S22** Fluorescence emission spectra of EtBr bounded to CT-DNA in the presence of **$PtL_2$**(a); [EtBr] = 20.0 µM, [CT-DNA] = 20.0 µM and [**$PtL_2$**] = 0 - 150 µM. The arrow shows the intensity changes upon increasing the **$PtL_2$** complex concentration. **(b)**: Stern-Volmer plot of $I_o/I$ versus [Q] and **(c)**: Scatchard plot of log[($I_o$–I)/$I$] versus log[Q].

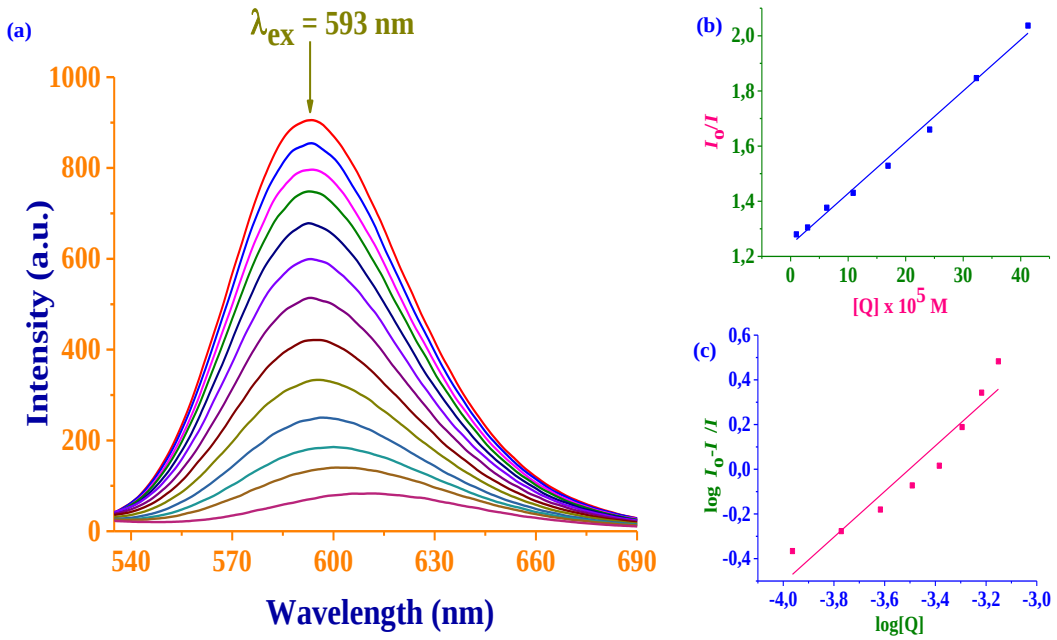


**Fig. S23** Fluorescence emission spectra of EtBr bounded to CT-DNA in the presence of **$PtL_3$**(a); [EtBr] = 20.0 µM, [CT-DNA] = 20.0 µM and [**$PtL_3$**] = 0-150 µM. The arrow shows the intensity changes upon increasing the **$Pt_3$** complex concentration. **(b)**: Stern-Volmer plot of $I_o/I$ versus [Q] and **(c)**: Scatchard plot of log[($I_o$–I)/$I$] versus log[Q].

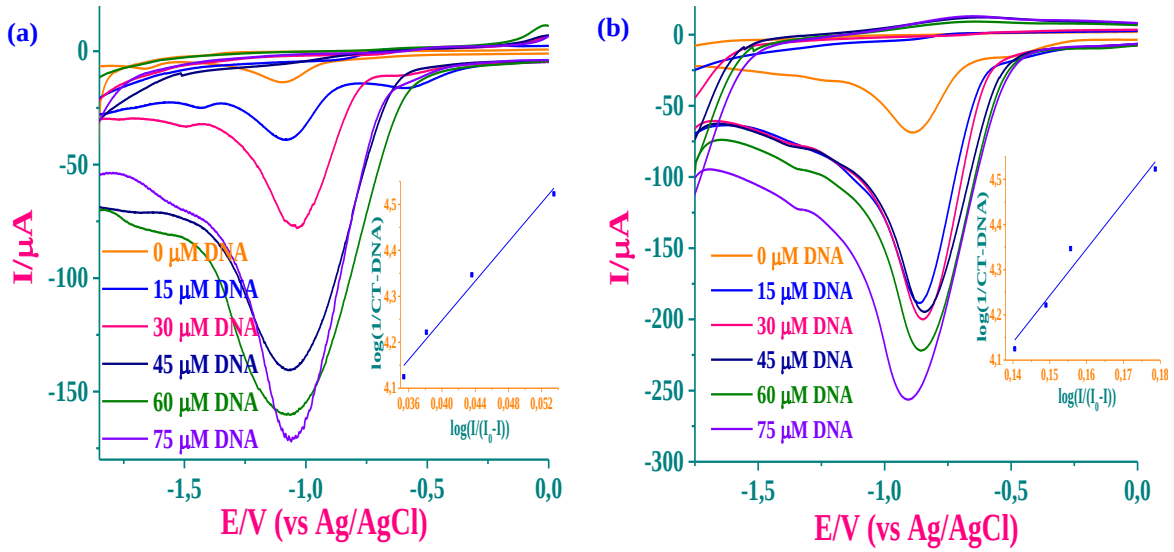


**Fig. S24** Cyclic voltammograms of 1.0 mM of **$PtL_2$** (a) and **$PtL_3$** (b) without and with CT-DNA at 100 mV/s.

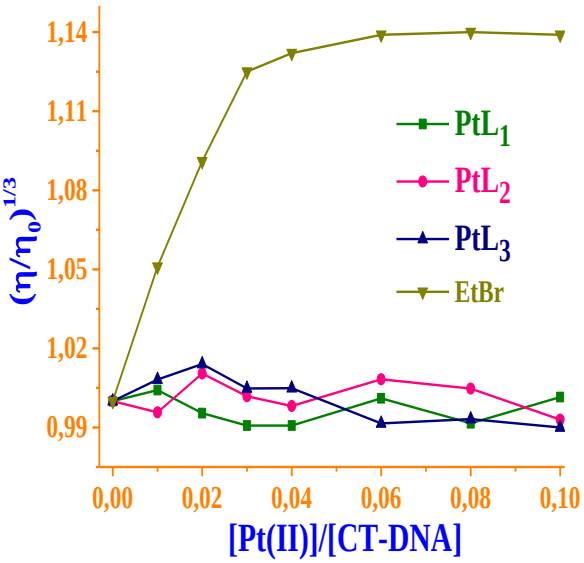


**Fig. S25** Effect of increasing amounts of **$PtL_1$**, **$PtL_2$**, **$PtL_3$** and EtBr on the relative viscosities of CT-DNA in 5 mM Tris-HCl/50 mM NaCl, pH 7.2.

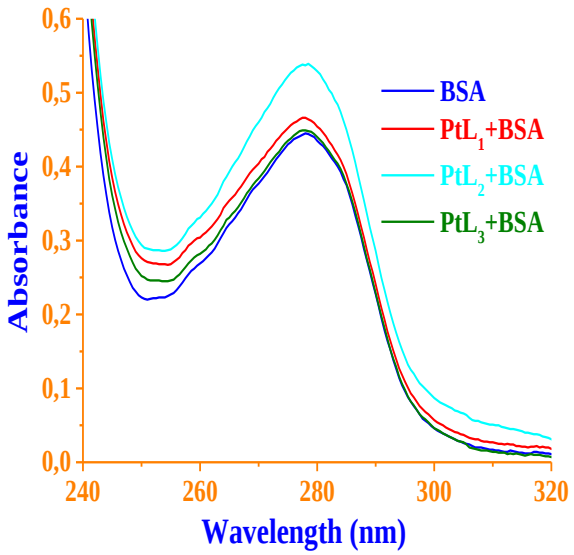


**Fig. S26** Absorption spectra of 10 µM BSA with and without 5 µM of each Pt(II) C^N^C pincer complex.

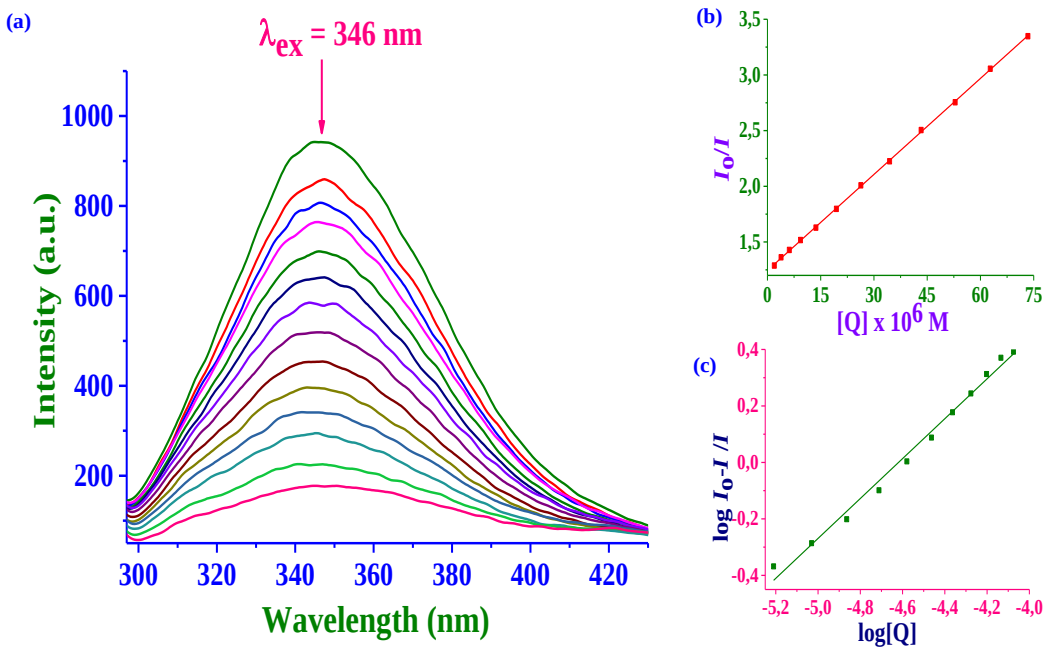


**Fig. S27** Fluorescence emission spectra of BSA in the absence and presence of **$PtL_2$**(a); [BSA] = 11.3 µM and [**$PtL_2$**] = 0 - 20 µM. The arrow shows the intensity changes upon increasing the **$PtL_2$** complex concentration. **(b)**: Stern-Volmer plot of $I_o/I$ versus [Q] and **(c)**: Scatchard plot of log[($I_o$–I)/$I$] versus log[Q].

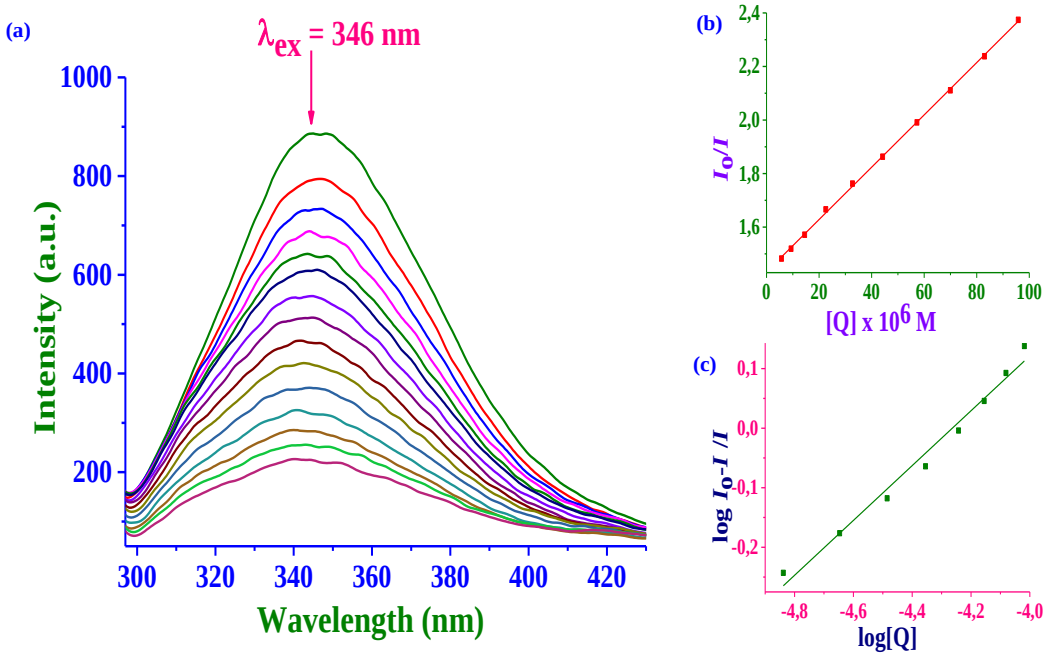


**Fig. S28** Fluorescence emission spectra of BSA in the absence and presence of **$PtL_3$**(a); [BSA] = 11.3 µM and [**$PtL_3$**] = 0 - 20 µM. The arrow shows the intensity changes upon increasing the **$PtL_3$** complex concentration. **(b)**: Stern-Volmer plot of $I_o/I$ versus [Q] and **(c)**: Scatchard plot of log[($I_o$–I)/$I$] versus log[Q].

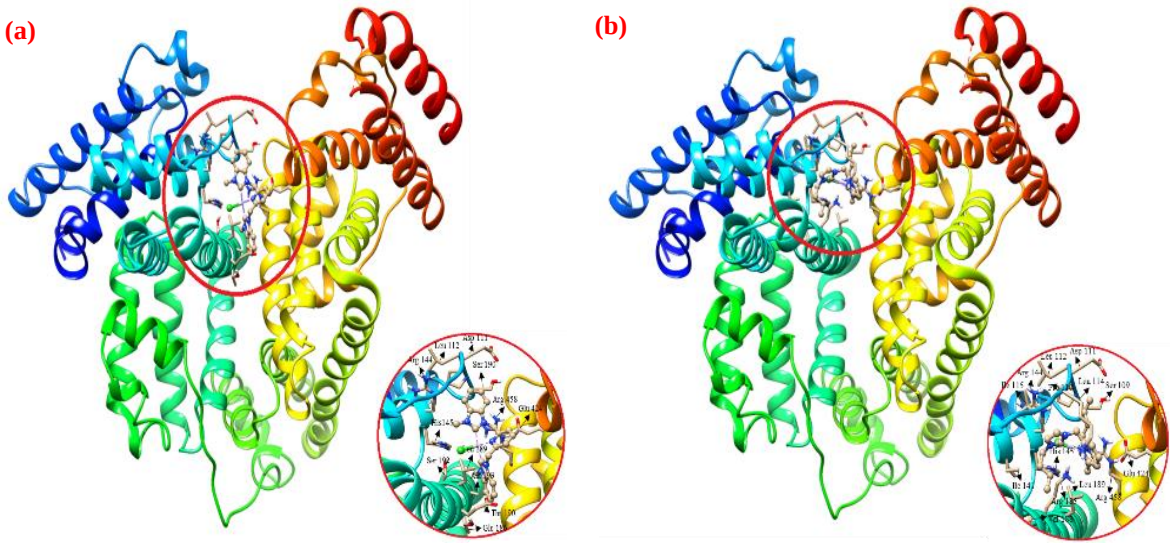


**Fig. S29** The lowest binding free energy conformers obtained between Pt(II) C^N^C pincer complexes (**$PtL_2$** (a) / **$PtL_3$** (b)) and BSA.

**Table S1** Summary of the second order rate constants, $k_2$ at 25, 45 and 55 °C for the substitution of aqua molecules by Nu.

| Complex | Nu | $k_2$ x $10^2$ / $M^{-1}$ $s^{-1}$ | | |
|---|---|---|---|---|
| | | 25 °C | 45 °C | 55 °C |
| 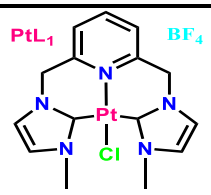 | tu | 2.20 ± 0.03 | 10.03 ± 0.08 | 20.96 ± 0.27 |
| | dmtu | 0.82 ± 0.02 | 6.41 ± 0.05 | 16.81 ± 0.21 |
| | Tmtu | 0.26 ± 0.01 | 0.74 ± 0.02 | 1.17 ± 0.04 |
| 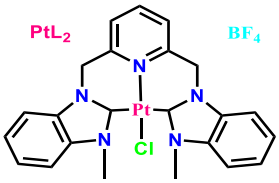 | tu | 1.34 ± 0.05 | 8.03 ± 0.7 | 17.44 ± 0.25 |
| | dmtu | 0.51 ± 0.03 | 4.19 ± 0.04 | 11.51 ± 0.16 |
| | Tmtu | 0.21 ± 0.01 | 0.63 ± 0.02 | 1.05 ± 0.03 |
| 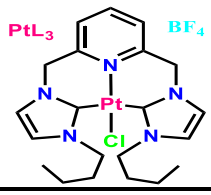 | tu | 0.33 ± 0.02 | 0.91 ± 0.03 | 1.42 ± 0.6 |
| | dmtu | 0.09 ± 0.01 | 0.43 ± 0.2 | 0.81 ± 0.3 |
| | Tmtu | 0.03 ± 0.01 | 0.13 ± 0.2 | 0.25 ± 0.2 |

**Table 2** DFT-calculated data for Pt(II) C^N^C pincer complexes

| **Complex** | **$PtL_1$** | **$PtL_2$** | **$PtL_3$** |
|---|---|---|---|
| MO energy (eV) | | | |
| $I = -E_{HOMO}$ | 6.772 | 6.829 | 6.691 |
| $A = -E_{LUMO}$ | 2.389 | 2.230 | 2.327 |
| $\Delta E_{LUMO-HOMO}$ | 4.383 | 4.600 | 4.364 |
| **NBO charge** | | | |
| $Pt^{2+}$ | 0.242 | 0.261 | 0.246 |
| $Cl^-$ | -0.454 | -0.451 | -0.453 |
| $N_{1=5}$ | -0.413 | -0.415 | -0.421 |
| $N_{2=4}$ | -0.430 | -0.435 | -0.430 |
| **Bond lengths (Å)** | | | |
| Pt-Cl | 2.445 | 2.443 | 2.442 |
| $Pt\text{-}N_{py}$ | 2.073 | 2.069 | 2.704 |
| $Pt\text{-}C_{1=2}$ | 2.048 | 2.046 | 2.050 |
| H····Cl | 2.694 | 2.702 | 2.051 |
| | | | |
| Electronegativity (χ) | 4.581 | 4.530 | 4.509 |
| Chemical softness (σ) | 0.456 | 0.435 | 0.458 |
| Chemical hardness (η) | 2.192 | 2.300 | 2.182 |
| Electrophilicity index (ω) | 4.787 | 4.461 | 4.659 |
| Dipole moment (D) | 12.705 | 12.368 | 13.722 |

**Table S3** Electrochemical potentials and current values of Pt(II) C^N^C pincer complexes with and without CT-DNA at scan rate 100 mV/s.

| **Complex, (1.0 mM)** | **$E_{pc}$, V** | | **Current, A** | |
|---|---|---|---|---|
| | **0 µM DNA** | **75 µM DNA** | **0 µM DNA** | **75 µM DNA** |
| **$PtL_1$** | -0.882 | -0.904 | $-6.87 \times 10^{-5}$ | $-2.56 \times 10^{-4}$ |
| **$PtL_2$** | -1.084 | -1.060 | $-4.48 \times 10^{-5}$ | $-1.92 \times 10^{-4}$ |
| **$PtL_3$** | -1.050 | -1.026 | $-1.36 \times 10^{-5}$ | $-1.72 \times 10^{-4}$ |